*Publ. Astron. Soc. Japan* (2015) 67 (4), 75 (1–9)
doi: 10.1093/pasj/psv042
Advance Access Publication Date: 2015 May 15

# Dark halos of M 31 and the Milky Way

**Yoshiaki SOFUE***

Institute of Astronomy, The University of Tokyo, 2-21-1 Osawa, Mitaka, Tokyo 181-0015, Japan

*E-mail: sofue@ioa.s.u-tokyo.ac.jp

Received 2015 February 2; Accepted 2015 April 21

## Abstract

Grand rotation curves (GRC) within ∼ 400 kpc of M 31 and the Milky Way were constructed by combining disk rotation velocities and radial velocities of satellite galaxies and globular clusters. The GRC for the Milky Way was revised using the most recent solar rotation velocity. The derived GRCs were deconvolved into a de Vaucouleurs bulge, exponential disk, and a dark halo with a Navarro–Frenk–White (NFW) density profile by least-$\chi^2$ fitting. Comparison of the best-fitting parameters revealed similarities between the disks and bulges of the two galaxies, whereas the dark-halo mass of M 31 was found to be twice that of the Galaxy. We show that the NFW model may be a realistic approximation of the observed dark halos in these two giant spirals.

**Key words:** Galaxy: fundamental parameters — Galaxy: structure — galaxies: dark matter — galaxies: individual (M 31) — galaxies: rotation curve

## 1 Introduction

The rotation curve of the Andromeda galaxy M 31 (NGC 224) has been obtained in detail and is used for determining the mass distribution in the disk and dark halo (Sofue et al. 1999; Carignan et al. 2006; Chemin et al. 2009; Corbelli et al. 2010). The dark-halo mass beyond the disk has been derived using kinematics of satellite galaxies (e.g., Metz et al. 2007; van der Marel & Guhathakurta 2008; Tollerud et al. 2012). Globular clusters are also used extensively for the mass determination of the dark halo (Veljanovski et al. 2014) as well as for inner kinematics (Galleti et al. 2004). In our recent work on the Milky Way Galaxy, we constructed a running averaged rotation curve for a wide region from the Galactic Center to the outermost dark halo, which we called the grand (or pseudo) rotation curve (hereafter, GRC; Sofue 2012, 2013). In the present paper, we revise the GRC by adopting the most recent value of the solar rotation velocity, $V_0 = 238\,\mathrm{km\,s^{-1}}$, from VERA observations (Honma et al. 2012).

We apply a common method to construct GRCs for M 31 and the Milky Way by combining disk rotation curves and radial velocities of satellite galaxies and outer globular clusters. We deconvolve the GRCs into bulge, disk, and dark halo, and determine the dynamical parameters. We compare the results for M 31 and the Milky Way, and discuss the similarities between the two galaxies. It is emphasized that the NFW model indeed works in largely extended dark halos of real galaxies.

## 2 Grand rotation curves

### 2.1 M 31

The rotation curve of the disk of M 31 has been obtained by many authors using H I, CO, and H$\alpha$ line kinematical data as listed in table 1. For the disk region, we simply adopt the averaged rotation velocity $V(R)$ as a function of radius $R$ from these data. For the halo region beyond the disk, we employ kinematics of non-coplanar objects orbiting M 31, which include satellite galaxies and globular clusters (table 1). We use a distance to M 31 of 770 kpc, and a systemic velocity of 300 km s$^{-1}$ (Courteau & van den Bergh 1999).

We assume that the distribution of non-coplanar objects is spherical around M 31 and the velocity vectors are

**Table 1.** References to the data in figure 1.

| | | |
|---|---|---|
| Rectangles at $R < 10$ kpc | Disk RC (CO) | Loinard, Allen, and Lequeux (1995) |
| Gray circles at $R < 32$ kpc | Ibid (combi: H I, CO, opt) | Sofue et al. (1981, 1999) |
| Gray open circles linked by line | Ibid (H I) | Carignan et al. (2006) |
| Black–gray circles linked by line | Ibid (H I, CO) | Chemin, Carignan, and Foster (2009) |
| Gray reverse triangles linked by line | Ibid (H I) | Corbelli et al. (2010) |
| Rectangles at $R > 40$ kpc | Galaxies around M 31 | Metz, Kroupa, and Jerjen (2007) |
| Triangles with bars | Ibid | van der Marel and Guhathakurta (2008) |
| Reverse triangle at $R > 40$ kpc | Ibid | Tollerud et al. (2012) |
| Open circles with bars | Globular clusters | Veljanovski et al. (2014) |

random. We define a pseudo rotation velocity, $V$, as the velocity that yields the enclosed mass $M(R)$ within a radius $R$ from the galaxy's center by

$$M(R) = V^2 R/G, \tag{1}$$

where $G$ is the gravitational constant. The pseudo rotation velocity is here replaced by the virial velocity for an ensemble of particles orbiting around the center of mass in random orbits (Limber & Mathews 1960; Bahcall & Tremaine 1981). If the orbits are random, the velocity is evaluated by

$$V = \sqrt{3\langle v_z^2 \rangle}, \tag{2}$$

where $v_z$ is the line-of-sight velocity of each object (Limber & Mathews 1960), and $\langle v_z^2 \rangle$ is the mean of the squares of $v_z$ in the ensemble. The factor $\sqrt{3}$ was multiplied for correction for the degree of freedom of random motion (Limber & Mathews 1960).

If the orbits are not random, the above estimation may be corrected for the orbital shapes by

$$V = C\sqrt{3\langle v_z^2 \rangle}. \tag{3}$$

Here, the coefficient $C$ is a factor ranging from $\sqrt{3}\pi/8 \sim 0.7$ for radial orbits to $3\pi/8 \sim 1.2$ for circular orbits (Bahcall & Tremaine 1981), depending on the shapes of the orbits as well as on the assumed potential and distribution function of objects (Evans et al. 2003).

Since it is rather the potential that we want to determine in this paper, and the other factors are unknown, we here assume that $C = 1$. It should be mentioned that the obtained result in this paper depends on this correction factor in the sense that the dark-halo mass is proporional to $C^2$. Namely, the mass could be changed by a factor of $\sim 2$. Hence, the given errors in this paper are statistical values, not considering the systematic effects of the assumption.

For objects whose three-dimensional coordinates are unknown, the distance from M 31's center $R$ is related to the projected distance $r_{\rm proj}$ by

$$R = \frac{\pi}{2} r_{\rm proj}. \tag{4}$$

We adopt the thus-calculated pseudo rotation velocity as the rotation velocity.

If there exists systematic rotation, as observed for the globular clusters around M 31 (Veljanovski et al. 2014), a correction is necessary, as described in the Appendix. We assume that the rotation axis is parallel to the disk's rotation axis, $i = 77°$, so that the correction is small and equation (3) also holds for the globular cluster system.

Figure 1 shows the compiled rotation velocities for the disk, and the pseudo rotation velocities of satellites and globular clusters within a radius of 500 kpc from M 31. Using these velocities, we calculate the running averaged

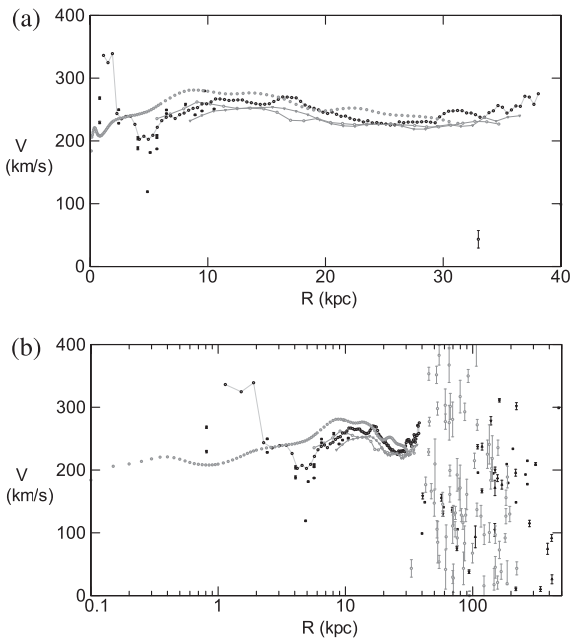


**Fig. 1.** Rotation velocities of the disk and pseudo rotation velocities of non-coplanar objects in M 31 in (a) linear and (b) semi-logarithmic scalings. References to the data are listed in table 1.

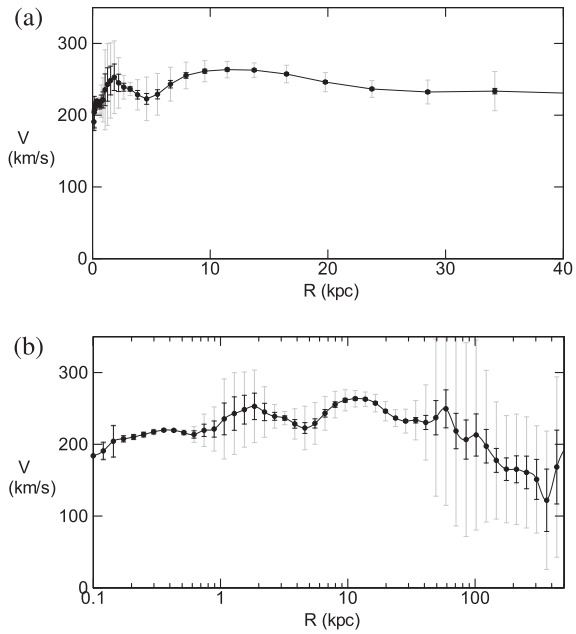


**Fig. 2.** GRC of M 31, showing running averaged values of pseudo rotation velocities in (a) linear and (b) logarithmic scalings. Long and short bars represent modified standard deviations and errors, respectively.

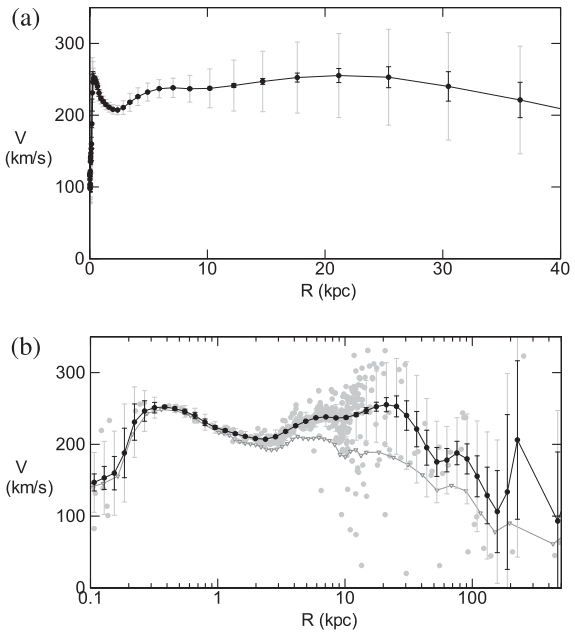


**Fig. 3.** New GRC of the Milky Way in (a) linear and (b) semi-logarithmic scalings. Gray dots represent the data for individual objects, and the gray line with triangles shows our earlier GRC (Sofue 2012, 2013).

velocities in each bin at logarithmic intervals between $R$ and $1.2\,R$ with $R$ starting from $R = 0.1$ kpc by applying the Gaussian running averaging procedure described in Sofue (2012, 2013). Note that we here use the root of the mean, $\sqrt{\langle v_z^2 \rangle}$, as the pseudo rotation velocity, because the squared velocity is more directly related to the virial mass according to equation (3), whereas we took $\langle v_z \rangle$ in the earlier work.

The pseudo rotation velocities are plotted in figure 2, where long bars represent modified standard deviations among the data used in each bin, and short bars are modified standard errors. Here, the modified deviation and error are defined by $s_d = \delta V \simeq \delta V^2/2V = s_{d:V^2}/2V$ and $s_e = s_{e:V^2}/2V$, recalling the propagation of the deviation (error) of $V^2$ and $V$ by the derivative relation $\delta V^2 = 2V\delta V$. Here, $s_{d:V^2} = [\langle (3v_z^2 - V^2)^2 \rangle]^{1/2}$ and $s_{e:V^2} = s_{d:V^2}/N^{1/2}$ are the standard deviation and error around $V^2$ in each radius bin, respectively, and $N$ is the number of data points in the bin.

We employed these definitions for the same reason that we chose the square value, $v_z^2$, as the independent variable, instead of the linear value, $v_z$. We call the thus-obtained plot of $V$ the grand rotation curve (GRC).

## 2.2 The Milky Way

We revise the GRC of the Milky Way obtained in our earlier work (Sofue 2013) by adopting the most recently determined value of the solar rotation velocity, $V_0 = 238\,\mathrm{km\,s^{-1}}$ at $R_0 = 8$ kpc, from VERA observations (Honma et al. 2012) in place of 200 km s$^{-1}$ in the earlier paper. We also adopt the same correction factor for velocity as for M 31, $V = \sqrt{3\langle v_z^2 \rangle}$, in place of $\sqrt{2}\langle v_z \rangle$. In the earlier work, the degree of freedom of motion was assumed to be 2, considering that each particle has a transverse velocity that is the same as the radial velocity.

The revised GRC is shown in figure 3, where the data used are superposed by gray dots, among which a few objects with $v_z \sim 400\,\mathrm{km\,s^{-1}}$ have been removed from the analysis. The new GRC exhibits higher velocities than our earlier result, shown by the gray line with triangles. The higher disk velocities are due to the use of the larger value of $V_0 = 238\,\mathrm{km\,s^{-1}}$, as well as to higher velocities for non-coplanar objects because of the use of the correction of $\sqrt{3}$ instead of $\sqrt{2}$. Also, the presently employed average of the squared velocity $v_z^2$ leads to a slightly higher mean velocity compared to the linear mean of $v_z$ in the previous work.

In figure 4 we compare the new GRC of the Milky Way with M 31. The two GRCs show a remarkable similarity in the halo regions, indicating similar dark-matter distributions.

## 2.3 Characteristics of the GRC

The general characteristics of the GRCs obtained for M 31 and the Galaxy may be summarized as follows:

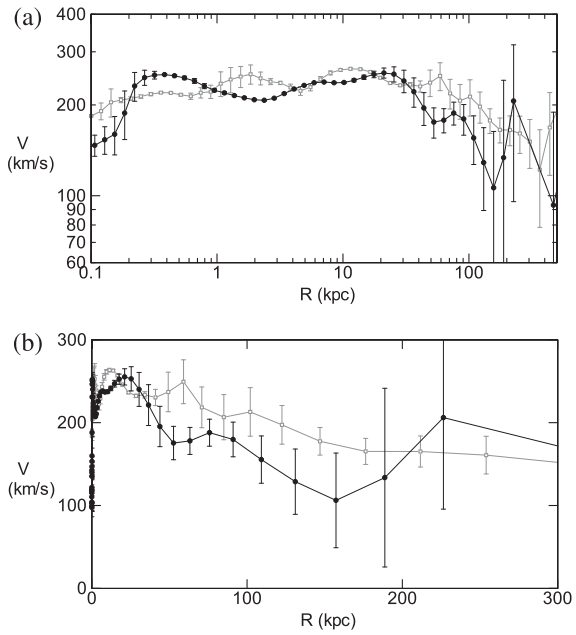


**Fig. 4.** New GRC of the Milky Way (solid line) compared with that of M31 (gray line) in (a) logarithmic and (b) linear scalings. The bars are modified standard errors.

(i) The rotation curves in the bulges look typical in the plot up to 40 kpc, but the enlarged curves in the logarithmic presentation show that they have inner structures. In particular, the innermost curve of the Milky Way was shown to be composed of multiple bulges with steeper concentrations than the de Vaucouleurs law predicts (Sofue 2013).

(ii) The disk rotation curves are nearly flat, showing broad maxima at $R \sim 10$–$20$ kpc in both galaxies.

(iii) Beyond $R \sim 30$ kpc the rotation velocity declines smoothly until the edge of the dark halo. The slope is, however, gentler than the Keplerian law predicts, implying that the halo cannot be represented by Plummer- or exponential-type potentials that require a steeper mass concentration. It will be shown in the next section that the NFW model is a good approximation to represent the observed GRCs in the halos.

## 3 Deconvolution of GRC into bulge, disk, and dark halo

We assume that the GRCs shown in figures 2 and 3 are composed of bulge, disk, and dark-halo contributions as

$$V(R)^2 = V_{\rm b}(R)^2 + V_{\rm d}(R)^2 + V_{\rm h}(R)^2, \tag{5}$$

where $V(R)$, $V_{\rm b}(R)$, $V_{\rm d}(R)$, and $V_{\rm h}(R)$ are the rotation velocity at galacto-centric distance $R$, and those for the bulge, disk, and dark halo, respectively. By fitting the GRC with a model rotation curve using the least-$\chi^2$ method, following the method presented by Sofue (2012, 2013), we searched for the best-fitting parameters of the bulge, disk, and dark halo.

### 3.1 Bulge

The bulge is assumed to have a de Vaucouleurs (1958) profile for the surface mass density as

$$\Sigma_{\rm b}(r) = \Sigma_{\rm be}\exp[-\kappa\{(r/a_{\rm b})^{1/4} - 1\}], \tag{6}$$

where $\kappa = 7.6695$ and $\Sigma_{\rm be}$ is the surface mass density at the half-mass scale radius $R = a_{\rm b}$. The total mass is calculated by

$$M_{\rm b} = 2\pi \int_0^\infty r\,\Sigma_{\rm b}(r)dr = \eta a_{\rm b}^2 \Sigma_{\rm be}, \tag{7}$$

with $\eta = 22.665$ being a dimensionless constant. The circular rotation velocity is then given by

$$V_{\rm b}(R) = \sqrt{GM_{\rm b}(R)/R}. \tag{8}$$

In the fitting procedure, $M_{\rm b}$ and $a_{\rm b}$ are taken as the two free parameters. The bulge of our Galaxy was shown to be composed of multiple bulges with exponential density profiles, whereas the de Vaucouleurs law rather fails to reproduce the innermost rotation curve (Sofue 2013). Hence, the present analysis will not be accurate enough for discussion of the bulge in the Milky Way.

### 3.2 Disk

The galactic disk is approximated by an exponential disk, whose surface mass density is expressed as

$$\Sigma_{\rm d}(R) = \Sigma_0 \exp\left(-R/a_{\rm d}\right), \tag{9}$$

where $\Sigma_0$ is the central value and $a_{\rm d}$ is the scale radius. The total mass of the exponential disk is given by

$$M_{\rm d} = \int_0^\infty 2\pi r\,\Sigma_{\rm d} dr = 2\pi\,\Sigma_0 a_{\rm d}^2. \tag{10}$$

The rotation curve for a thin exponential disk is expressed by

$$V_{\rm d}(R) = \sqrt{GM_{\rm d}/a_{\rm d}}\,\mathscr{D}(X), \tag{11}$$

where $X = R/a_{\rm d}$, and $\mathscr{D}(X)$ is the expression obtained by Freeman (1970) for a flat exponential disk. As the two free parameters we chose $M_{\rm d}$ and $a_{\rm d}$.

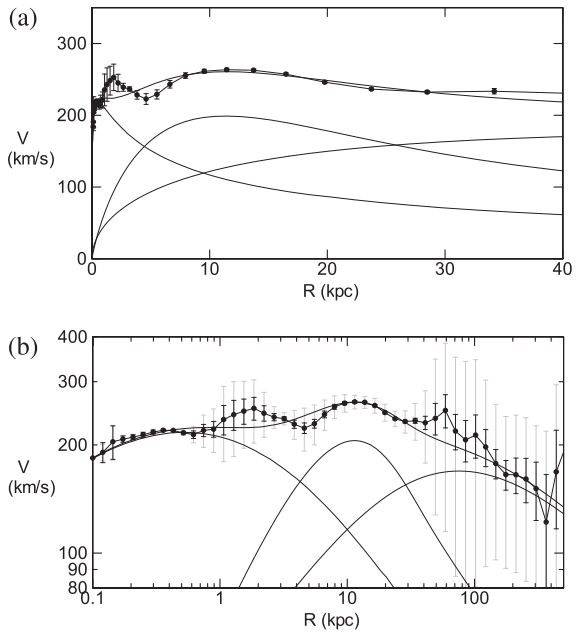


**Fig. 5.** Least-$\chi^2$ fit of the GRC of M 31 by the bulge, disk, and dark-halo components in (a) linear and (b) logarithmic scalings.

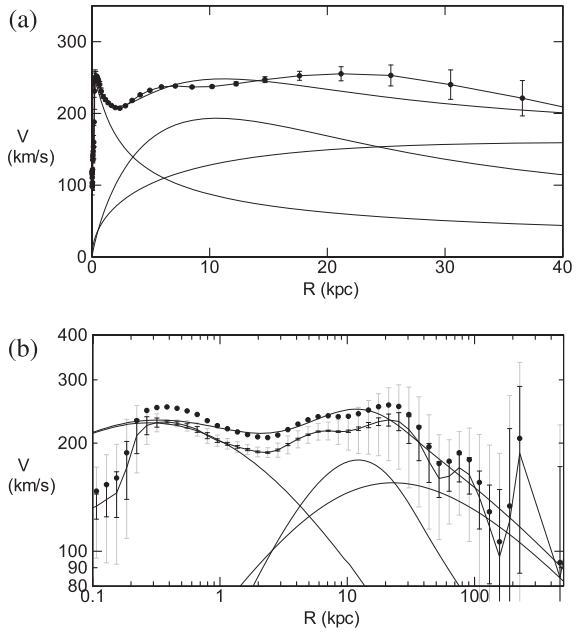


**Fig. 6.** Same as figure 5, but for the revised new GRC of the Milky Way using the same procedure as for M 31.

### 3.3 Dark halo

For the dark halo, three mass models have so far been proposed: the semi-isothermal (Begeman et al. 1991), NFW (Navarro et al. 1996), and Burkert (1996) models. The outermost rotation curves in figures 5 and 6 are not flat at all, so the isothermal model is not a good approximation. Since the NFW and Burkert models are essentially the same except for the very central part, we here adopt the NFW profile. The NFW density profile is expressed as

$$\rho(R) = \rho_0/[X(1+X)^2], \tag{12}$$

where $X = R/h$, and $\rho_0$ and $h$ are the representative (scale) density and scale radius of the dark halo, respectively. In the fitting procedure, we chose $\rho_0$ and $h$ as the two free parameters.

The enclosed mass within radius $R$ is given by

$$M_{\rm h}(R) = 4\pi\rho_0 h^3 \left\{\ln(1+X) - X/(1+X)\right\}. \tag{13}$$

The circular rotation velocity is given by

$$V_{\rm h}(R) = \sqrt{GM_{\rm h}(R)/R}. \tag{14}$$

### 3.4 Fitting result by the least-$\chi^2$ method

Applying the fitting method described in Sofue (2012) to the GRC of M 31 and the Galaxy, we searched for the best-fitting parameters of the bulge, disk, and dark halo. The free parameters are $M_{\rm b}$, $a_{\rm b}$, $M_{\rm d}$, $a_{\rm d}$, $\rho_0$, and $h$. Fitting radii were taken to be $R_1 = 0$ to $R_2 = 20$ kpc for the bulge, 0–40 kpc for disk, and 1–385 kpc for the dark halo. The outer boundary for the halo fitting corresponds to the half distance between the two galaxies. Figures 5 and 6 show the thus-obtained fitting results compared with the GRCs used. Table 2 shows the best-fitting parameters for the individual mass components.

Figures 7 and 8 show the behaviors of $\chi^2/N$ around the least values, where $\chi$ is defined by $\chi^2 = \Sigma[V_{\rm c}(R_i)^2 - V_{\rm o}(R_i)^2]/s_d^2$, with "o" and "c" standing for the observed and calculated values, respectively, and $N$ is the number of fitting points. For the dark halo we present the total dark mass, $M_{\rm h:385}$, corresponding to $h$ and $\rho_0$. Since the fitting areas and $N$ for the bulge, disk, and halo are different, the minimum $\chi$ values differ between the components. The error of each fitted parameter was evaluated as the range that allows for an increase of the $\chi^2$ value by 10% above the least value.

## 4 Discussion

### 4.1 Summary

We constructed GRCs of the Andromeda galaxy M 31 and the Milky Way Galaxy for wide regions from the centers to the dark-halo edges (figures 2 and 3). The GRC for the Milky Way was revised by adopting the most recent solar rotation velocity and applying the same method as for M 31.

**Table 2.** The best-fitting dynamical parameters for M 31 and the Galaxy.

| Component | Parameter* | M 31 | Milky Way |
|---|---|---|---|
| Bulge | $a_b$ (kpc) | 1.35 ± 0.02 | 0.87 ± 0.07 |
| | $M_b$ ($10^{11}\,M_\odot$) | 0.35 ± 0.004 | 0.25 ± 0.02 |
| Disk | $a_d$ (kpc) | 5.28 ± 0.25 | 5.73 ± 1.23 |
| | $M_d$ ($10^{11}\,M_\odot$) | 1.26 ± 0.08 | 1.12 ± 0.40 |
| NFW halo | $h$ (kpc) | 34.6 ± 2.1 | 10.7 ± 2.9 |
| | $\rho_0$ ($10^{-3}\,M_\odot\,\mathrm{pc}^{-3}$) | 2.23 ± 0.24 | 18.2 ± 7.4 |
| | $\rho_{8\mathrm{kpc}}$ ($10^{-3}\,M_\odot\,\mathrm{pc}^{-3}$) | 6.36 ± 0.70 | 7.93 ± 3.24 |
| | = (in energy density: GeV cm$^{-3}$) | 0.24 ± 0.03 | 0.30 ± 0.12 |
| | $M_{h:200}$ ($10^{11}\,M_\odot$) | 12.3 ± 2.6 | 5.7 ± 5.1 |
| | $M_{h:385}$ ($10^{11}\,M_\odot$) | 18.3 ± 3.9 | 7.3 ± 6.7 |
| Total mass | $M_{tot:200}$ ($10^{11}\,M_\odot$) | 13.9 ± 2.6 | 7.0 ± 5.1 |
| | $M_{tot:385}$ ($10^{11}\,M_\odot$) | 19.9 ± 3.9 | 8.7 ± 5.1 |
| Bulge | $\chi^2_b/N$ ($R_1$–$R_2$ kpc) | 0.36 (0.0–20.0) | 3.5 (0.0–20.0) |
| Disk | $\chi^2_d/N$ ($R_1$–$R_2$ kpc) | 0.33 (0.0–40.0) | 3.6 (0.0–40.0) |
| Halo | $\chi^2_h/N$ ($R_1$–$R_2$ kpc) | 0.25 (0.0–385.0) | 3.0 (0.0–385.0) |

*$M_{h:200}$, $M_{h:385}$, $M_{tot:200}$, and $M_{tot:385}$ are dark-halo and total masses within $R = 200$ and 385 kpc, respectively; $\rho_{8\mathrm{kpc}}$ is a local value at $R = 8$ kpc both in mass and energy densities; $R_1$ and $R_2$ are start and end radii for fitting.

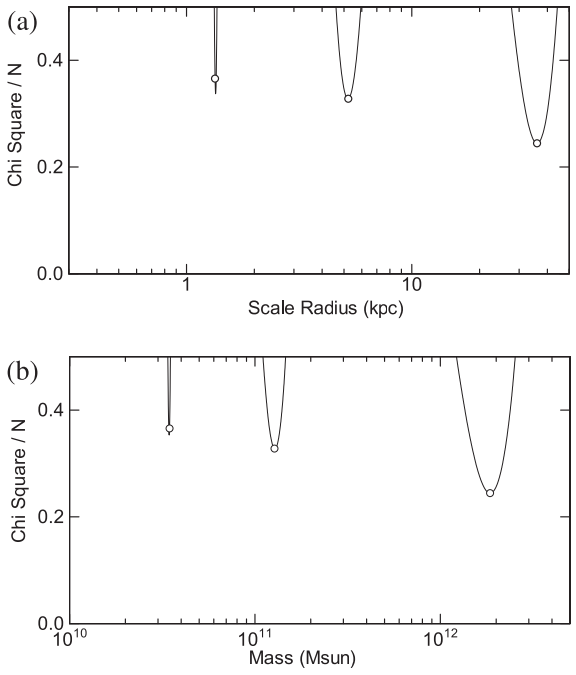


**Fig. 7.** (a) Values of $\chi^2/N$ for M 31 as functions of $a_b$, $a_d$, and $h$ around the least values marked by circles. From left to right: bulge, disk, and dark halo, respectively. (b) Same as (a), but for the masses $M_b$, $M_d$, and $M_{h:385}$.

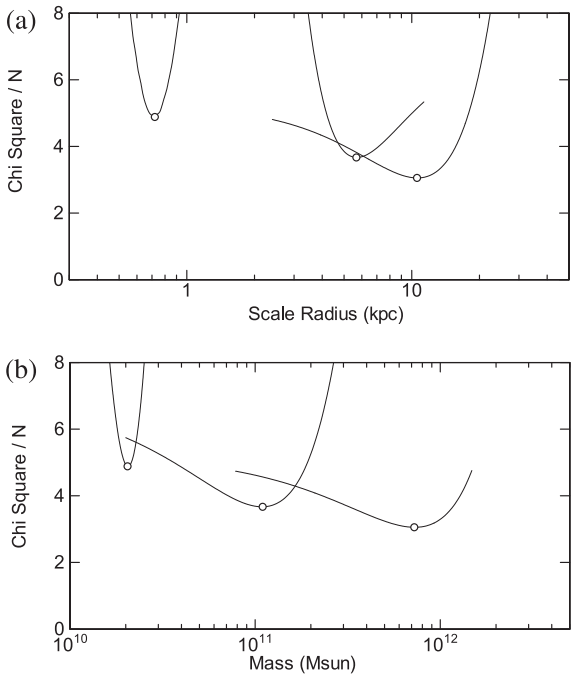


**Fig. 8.** Same as figure 7, but for the Milky Way using the newly determined revised GRC.

As stressed below, the dark halos of both galaxies are well represented by the NFW density profiles.

By least-$\chi^2$ fitting to the obtained GRCs up to a radius of 385 kpc (figures 5 and 6), we determined the galactic parameters for the bulge, disk, and dark halo, as listed in table 2. Our result for M 31 is consistent with those obtained by other authors in recent years, as compared in table 3 and figure 10.

**Table 3.** Comparison of the derived dark-halo and total masses of M 31 with other works in recent years.

| Author | Mass | in $10^{11}\,M_\odot$ |
|---|---|---|
| Evans et al. (2003) | $M_{\rm tot:100}$ | 7–10 |
| Ibata et al. (2004) | $M_{\rm tot:125}$ | $7.5 \pm 1.3$ |
| Geehan et al. (2006) | $M_{\rm h:200}{}^*$ | 7.1 |
| Seigar, Barth, and Bullock (2008) | $M_{\rm h:200}{}^*$ | 7.3 |
| Lee et al. (2008) | $M_{\rm tot:100}$ | $19.0 \pm 1.3$ |
| Chemin, Carignan, and Foster (2009) | $M_{\rm h:160}$ | 10.0 |
| Corbelli et al. (2010) | $M_{\rm h:200}{}^*$ | $13 \pm 3$ |
| Watkins, Evans, and An (2010) | $M_{\rm tot:300}$ | $14 \pm 4$ |
| van der Marel et al. (2012) | $M_{\rm tot:Vir(385)}$ | $17.2 \pm 2.5$ |
| Tollerud et al. (2012) | $M_{\rm tot:139}$ | $8 \pm 4$ |
| Tamm et al. (2012) | $M_{\rm h:200}{}^*$ | 11.3–12.7 |
| Fardal et al. (2013) | $M_{\rm tot:200}$ | $20 \pm 5$ |
| Veljanovski et al. (2014) | $M_{\rm h:200}{}^*$ | 12–16 |
| This work (2015) | $M_{\rm h:200}{}^*$ | $12.3 \pm 2.6$ |
| – | $M_{\rm h:385}$ | $18.3 \pm 3.9$ |
| – | $M_{\rm tot:200}$ | $13.9 \pm 2.6$ |
| – | $M_{\rm tot:385}$ | $19.9 \pm 3.9$ |
| Average $\langle M_{\rm h:200}\rangle^*$ | | $11 \pm 3$ |
| Average $\langle M_{\rm tot:100\,-\,385}\rangle$ | | $14 \pm 5$ |

*Dark matter mass within radius 200 kpc.

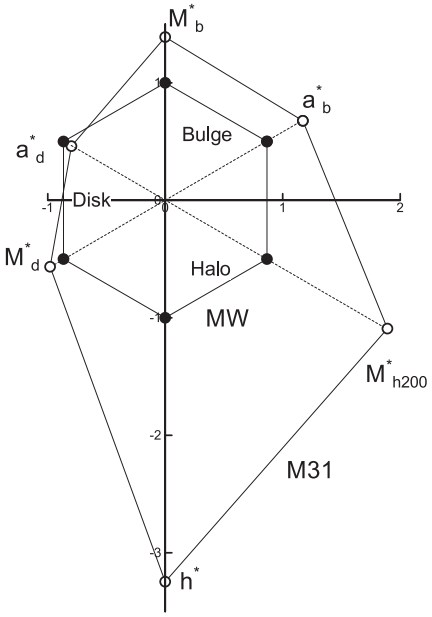


**Fig. 9.** Comparison of the dynamical parameters of M 31 (open circles) relative to those of the Milky Way (filled circles). The quantities marked with asterisks show the values relative to those of the Milky Way.

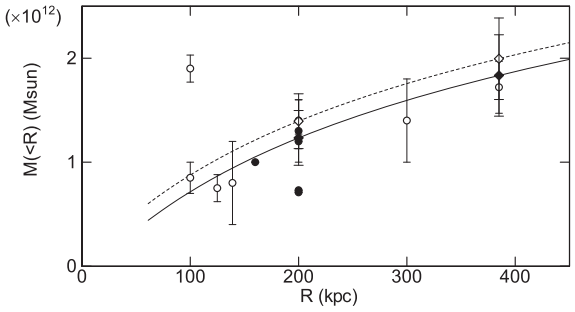


**Fig. 10.** Enclosed dark (filled) and total masses (open circles) within $R$ of M 31 obtained by the authors listed in table 3. Upper (dashed) and lower (solid) lines show $M_{\rm tot}(R)$ and $M_{\rm h}(R)$, respectively, calculated using the fitted parameters of M 31. Big diamonds on the calculated lines indicate the present result.

## 4.2 The reality of the NFW model

The fitting result in figures 5 and 6 proves that the NFW profile (Navarro et al. 1996) can be a realistic approximation to represent the observed dark halos. We emphasize that the analysis of GRCs covering regions as wide as several hundred kpc around the galaxies is essential to identify the right model from the three types of dark-halo models: the isothermal model, predicting flat rotation in the outermost region as $V_{\rm rot} \propto$ const; the NFW model, predicting slowly decreasing rotation as $\propto (\ln R/R)^{-1/2}$; and Plummer- or exponential-type models, predicting Keplerian decrease as $\propto R^{-1/2}$ at large radii.

## 4.3 Similarities between the GRCs in M 31 and the Milky Way and differences in the dark-halo masses

In figure 4 the GRC of M 31 is compared with the revised GRC of the Milky Way, and the fitting results are compared in table 2. There is a remarkable similarity between the rotation curves inside the disk regions as well as in the dark halos in their shapes and amplitudes. However, the fitted dark-halo mass of M 31 is about twice that of the Galaxy and the parameters are also different, although the bulge and disk parameters are similar between the two galaxies. Figure 9 compares the fitted parameters of M 31 relative to those of the Milky Way.

## 4.4 Revised GRC of the Milky Way

The fitting accuracy in the Milky Way is not satisfactory, particularly for the bulge component (figure 8), which is mainly due to the fact that the Galactic bulge is composed of multiple components, not well represented by the de Vaucouleurs law (Sofue 2013). However, we used the common model for M 31 in order to compare the global structures of the two galaxies. Hence, the innermost structure of the Milky Way may not be taken seriously here, while it does not affect the result for the disk and dark halo.

The scale radii and masses for the Milky Way determined here are systematically greater than those obtained in our previous work (Sofue 2013). This is because of the use of the larger rotation velocity of the Sun, which causes a significant increase in the disk rotation velocities, as well as changing the revised correction factor of radial velocities of non-coplanar objects.

### 4.5 Baryonic fraction

The ratio of the total mass of the bulge and disk to the dark-matter mass, $\Gamma = (M_{\rm b} + M_{\rm d})/M_{\rm h:385}$, is a measure of the baryonic-to-dark-mass ratio. The values in table 2 yield a ratio of $\Gamma \sim 0.087$ for M 31, and 0.25 for the Galaxy. These values may be compared with the cosmological value of 0.19 (= 4.5%/24%) from the WMAP observations (Spergel et al. 2003). This implies that M 31 is dark-matter dominant compared to the cosmological value, whereas the Galaxy is baryon exceeded.

### 4.6 Relation to the Local Group

The systemic velocity of M 31 with respect to the Milky Way of $\sim 100\,{\rm km\,s^{-1}}$ (Courteau & van den Bergh 1999) can be translated to a statistically possible mutual velocity by multiplying $\sqrt{3}$ to yield $\sim 170\,{\rm km\,s^{-1}}$, if we assume that the two galaxies' motions are random. In order for the two galaxies to be bound, the reduced total mass of the whole system is required to be greater than $\sim 5 \times 10^{12}\,M_\odot$. Since both M 31 and the Galaxy are far less massive, $\sim 3 \times 10^{12}\,M_\odot$ in total, than this binding mass, there remain two possibilities: either the Local Group contains dark mass as massive as $\sim 2 \times 10^{12}\,M_\odot$, or the two galaxy systems are not gravitationally bound.

In the former case, our view that the Local Group can be recognized as one system may not be changed. However, the dark mass must be concentrated around the center of mass of the Local Group, so that the M 31 and the Galaxy groups, both associated with their own dark halos and embedded satellite galaxies and globular clusters, are not tidally disrupted.

In the latter possibility, we need no further assumption of dark mass in the Local Group, but it is required that M 31 and the Galaxy and their satellite galaxies have been two individual bound systems since formation. In fact, Sawa and Fujimoto (2005) proposed a model in which dwarf galaxies of the Local Group are bound either to M 31 or the Milky Way, composing two individual bound groups, and the two groups are orbiting around each other and tidally interacting.

## Appendix 1. Pseudo rotation velocity in a pressure-supported rotating system

If there exists systematic rotation $V_{\rm rot}$ in the halo, the velocity $V = |V|$ of a satellite galaxy and/or globular cluster (hereafter, particle) is expressed as

$$V^2 = (\boldsymbol{V}_{\rm rot} + \boldsymbol{V}_{\rm ran})^2 = V_{\rm rot}^2 + 2\boldsymbol{V}_{\rm rot}\cdot\boldsymbol{V}_{\rm ran} + V_{\rm ran}^2, \tag{A1}$$

where $\boldsymbol{V}_{\rm ran}$ is the velocity corresponding to the pressure-support term. When $V^2$ is averaged around the galaxy, the crossing term disappears because of the randomness of $\boldsymbol{V}_{\rm ran}$ and axisymmetry of $\boldsymbol{V}_{\rm rot}$, yielding

$$\langle V^2\rangle = \langle V_{\rm rot}^2\rangle + \langle V_{\rm ran}^2\rangle. \tag{A2}$$

The first term is related to the apparent rotation velocity projected on the sky, $v_{z:{\rm rot}}$, as

$$v_{z:{\rm rot}} = V_{\rm rot}\sin i\cos\theta. \tag{A3}$$

Here, $i$ is the inclination angle of the rotation axis, and $\theta$ is the azimuthal angle of the particle from the major axis. Knowing that $i$ and $\theta$ are independent and $\langle\cos^2\theta\rangle = 1/3$ by averaging over $\theta$ from 0 to $\pi/2$, we have

$$\langle V_{\rm rot}^2\rangle = \frac{3}{\sin^2 i}\langle v_{z:{\rm rot}}^2\rangle. \tag{A4}$$

Replacing $\langle V_{\rm ran}^2\rangle$ by $3\langle v_{z:{\rm ran}}^2\rangle$, where $v_{z:{\rm ran}}$ is the $z$-directional component of $\boldsymbol{V}_{\rm ran}$, we obtain

$$\langle V^2\rangle = 3\langle v_{z:{\rm ra}}^2\rangle + \frac{3}{\sin^2 i}\langle v_{z:{\rm rot}}^2\rangle. \tag{A5}$$

Writing the observable $z$-directional velocity as $v_z = v_{z:{\rm ran}} \pm v_{z:{\rm rot}}$, and remembering that the crossing term $\langle\pm 2 v_{z:{\rm ran}} v_{z:{\rm rot}}\rangle$ reduces to zero for randomness of the sign of $v_{z:{\rm ran}}$, we obtain

$$\langle v_z^2\rangle = \langle v_{z:{\rm ra}}^2\rangle + \langle v_{z:{\rm rot}}^2\rangle. \tag{A6}$$

Hence, we have

$$\langle V^2\rangle = 3\langle v_z^2\rangle + 3\cot^2 i\,\langle v_{z:{\rm rot}}^2\rangle. \tag{A7}$$

For an edge-on case, $i = 90^\circ$, we have

$$\langle V^2\rangle = 3\langle v_z^2\rangle, \tag{A8}$$

the same as for random motion (Limber & Mathews 1960). If we assume the same inclination as the main disk of M 31, $i = 77^\circ$ to $78^\circ$, we have

$$\langle V^2\rangle = 3\langle v_z^2\rangle + \alpha\langle v_{z:{\rm rot}}^2\rangle \tag{A9}$$

with $\alpha \simeq 0.15$. Since $\langle v_{z:\mathrm{rot}}^2 \rangle$ is smaller than $\langle v_z^2 \rangle$, we may neglect the second term, obtaining

$$\langle V^2 \rangle \simeq 3 \langle v_z^2 \rangle. \tag{A10}$$

Finally, we define the pseudo rotation velocity as

$$V = \sqrt{\langle V^2 \rangle} = \sqrt{3 \langle v_z^2 \rangle}. \tag{A11}$$

## References


Bahcall, J. N., & Tremaine, S. 1981, ApJ, 244, 805
Begeman, K. G., Broeils, A. H., & Sanders, R. H. 1991, MNRAS, 249, 523
Burkert, A. 1995, ApJ, 447, L25
Carignan, C., Chemin, L., Huchtmeier, W. K., & Lockman, F. J. 2006, ApJ, 641, L109
Chemin, L., Carignan, C., & Foster, T. 2009, ApJ, 705, 1395
Corbelli, E., Lorenzoni, S., Walterbos, R., Braun, R., & Thilker, D. 2010, A&A, 511, A89
Courteau, S., & van den Bergh, S. 1999, AJ, 118, 337
de Vaucouleurs, G. 1958, ApJ, 128, 465
Evans, N. W., Wilkinson, M. I., Perrett, K. M., & Bridges, T. J. 2003, ApJ, 583, 752
Fardal, M. A., et al. 2013, MNRAS, 434, 2779
Freeman, K. C. 1970, ApJ, 160, 811
Galleti, S., Federici, L., Bellazzini, M., Fusi Pecci, F., & Macrina, S. 2004, A&A, 416, 917
Geehan, J. J., Fardal, M. A., Babul, A., & Guhathakurta, P. 2006, MNRAS, 366, 996
Honma, M., et al. 2012, PASJ, 64, 136
Ibata, R., Chapman, S., Ferguson, A. M. N., Irwin, M., Lewis, G., & McConnachie, A. 2004, MNRAS, 351, 117
Lee, M. G., Hwang, H. S., Kim, S. C., Park, H. S., Geisler, D., Sarajedini, A., & Harris, W. E. 2008, ApJ, 674, 886
Limber, D. N., & Mathews, W. G. 1960, ApJ, 132, 286
Loinard, L., Allen, R. J., & Lequeux, J. 1995, A&A, 301, 68
Metz, M., Kroupa, P., & Jerjen, H. 2007, MNRAS, 374, 1125
Navarro, J. F., Frenk, C. S., & White, S. D. M. 1996, ApJ, 462, 563
Sawa, T., & Fujimoto, M. 2005, PASJ, 57, 429
Seigar, M. S., Barth, A. J., & Bullock, J. S. 2008, MNRAS, 389, 1911
Sofue, Y. 2012, PASJ, 64, 75
Sofue, Y. 2013, PASJ, 65, 118
Sofue, Y., & Kato, T. 1981, PASJ, 33, 449
Sofue, Y., Tutui, Y., Honma, M., Tomita, A., Takamiya, T., Koda, J., & Takeda, Y. 1999, ApJ, 523, 136
Spergel, D. N., et al. 2003, ApJS, 148, 175
Tamm, A., Tempel, E., Tenjes, P., Tihhonova, O., & Tuvikene, T. 2012, A&A, 546, A4
Tollerud, E. J., et al. 2012, ApJ, 752, 45
van der Marel, R. P., Fardal, M., Besla, G., Beaton, R. L., Sohn, S. T., Anderson, J., Brown, T., & Guhathakurta, P. 2012, ApJ, 753, 8
van der Marel, R. P., & Guhathakurta, P. 2008, ApJ, 678, 187
Veljanovski, J., et al. 2014, MNRAS, 442, 2929
Watkins, L. L., Evans, N. W., & An, J. H. 2010, MNRAS, 406, 264